RSC Advances

ROYAL SOCIETY OF CHEMISTRY

www.rsc.org/advances

Journal Name

RSCPublishing

COMMUNICATION

Mesoporous $ZnCo_2O_4$ microspheres as anode material for high-performance secondary lithium ion batteries

Cite this: DOI: 10.1039/x0xx00000x

Lingyun Guo,[a, b, c] Qiang Ru, [*, a, b, c] Xiong Song,[a, b, c] Shejun Hu,[a, b, c] Yudi Mo,[a, b, c]

Received ooth xxxx xxxx,
Accepted ooth xxxx xxxx

DOI: 10.1039/x0xx00000x

www.rsc.org/

Herein, the mesoporous $ZnCo_2O_4$ microspheres is fabricated by a facile hydrothermal method followed by pyrolysis of the $Zn_{0.33}Co_{0.67}CO_3$ precursor. The obtained $ZnCo_2O_4$ microspheres is made up of closely packed primary nanoparticles with diameter of about 30 nm and a large amount pores with the size ranging from 10 to 40 nm, which results in the high BET surface area of 39.52 m^2 g^{-1}. The large surface area permits a high interfacial contact area with the electrolyte and provides more locations and channels for fast Li^+ into insertion/extraction into the electrode material. The porous structure may not only be beneficial for Li^+ ion to diffuse efficiently to active material with less resistance but also buffer the volume expansion during the discharge/charge process. When used as an anode material, the specific capacity maintains a high value of 1256 mAh g^{-1} after 100 cycles at a current density of 100 mA g^{-1}, which is about 3.4 times larger than that of the commercial graphite electrode (372 mAh g^{-1}). More interesting, the reversible capacity as high as 774 mAh g^{-1} can be retained at a high current density of 1000 mA g^{-1} after 200 cycles, which indicates that the mesoporous $ZnCo_2O_4$ microspheres have excellent cycling performance at a high current density as anode materials for LIBs.

Introduction

Nowadays, Lithium ion batteries are the biggest concern secondary batteries that serve as recharge power source for portable electronic and high energy areas because of their high energy density, long lifespan and environmentally friendly. [1-4] However, a theoretical capacity of commercial graphite electrodes is only 372 mAh g^{-1}, which cannot meet the increasing demand for high energy density. [5] As a result, a large amount of efforts are made to design and prepared various material as anode material for LIBs, such as Si, [6] Sn, [7] carbon, [8] transition metal oxides [9, 10] and so on. Among them, transition metal oxides with nanostructured have attracted extremely interest due to their promising electrical properties, such as NiO,[11] Fe_2O_3,[12] Co_3O_4[13]. Based on previous reports on electrochemical performance of transition metal oxides, Co_3O_4 has shown the best anodic performance. [14] However, Co_3O_4 is not an ideal electrode material due to its toxicity and high cost. Thus, combination of two transition metal oxides with the spinel structure of ACo_2O_4 (A= Zn, Cu, Fe, Mg, Ni), [15-20] has been investigated immensely and considered as ideal anodic materials because of the complementarities and synergies between metal elements in the cycle process. For example, $NiCo_2O_4$ shows better electronic conductivity and better electrochemical activity than either nickel oxide or cobalt oxide. [21]

However, it is well known that the huge volume changes arising from the conversion reaction mechanism during the cycle process, would lead to the pulverization of electrode materials and detachment from the current collector, resulting in poor cyclability. Therefore, various structures with different shapes, such as nanotubes, nanorods, nanowires, nanophase, etc [22-30], were synthetized to resolve the volume expansion. It could be conclude that porous nanostructure with nanosize regions or domains appear the excellent electrochemical performance because of enough free space and high specific surface area. The high specific surface area and nanosize structure have many advantages, including improved cycling life, high effective contact areas, shorten path length and so on. [31, 32] Furthermore, the free space can serve as buffer space during lithium ion insertion and extraction.

In this paper, the mesoporous $ZnCo_2O_4$ microspheres was prepared directly by a typical hydrothermal method. The whole experimental flowchart is schematically illustrated in Fig. 1.

Frist, $Zn_{0.33}Co_{0.67}CO_3$ microspheres as the precursor was obtained by a facile solvothermal process. Afterwards, the precursor was calcined under air atmosphere to turn into the mesoporous $ZnCo_2O_4$ microspheres with escaping CO_2 gas. When used as electrode materials for LIBs, the Li^+ ion could pass into the $ZnCo_2O_4$ microspheres with little resistance and short distance due to the existence of pores. Thus, the mesoporous $ZnCo_2O_4$ microspheres is predicted to show high reversible specific capacities, good cyclability and excellent rate performance as anode materials for LIBs.

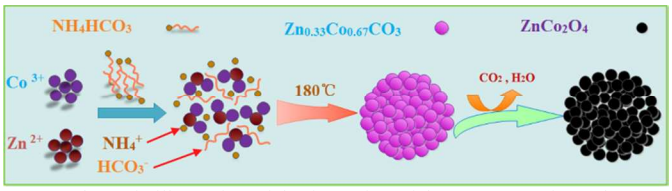

Fig. 1 Schematic illustration of the formation of the $ZnCo_2O_4$ microspheres

Experimental

Material synthesis

The mesoporous $ZnCo_2O_4$ microspheres prepared directly by a typical hydrothermal method. In a typical synthesis, 1mmol zinc nitrate ($Zn(NO_3)_2$•$6H_2O$, Aladdin, 99.9%) and 2mmol cobalt chloride ($CoCl_2$•$6H_2O$, Aladdin, 99.9%) were dissolved into a mixed solution containing ethylene glycol (EG 25ml) and distilled water (25ml) under magnetic stirring at first. Then, 30mmol of ammonium bicarbonate (NH_4HCO_3) as complex agent was added to the above mixture solution with continually stirring for 40 min, which resulted in a clear mixture solution. The clear solution was transferred into a Teflon lined stainless-steel autoclave (100ml capacity) and maintained at 180 ℃ for 20 h. The pink precipitate was collected and washed with distilled water and absolute alcohol for several times and dried at 60 ℃ for 6 h. To obtain the mesoporous $ZnCo_2O_4$ microspheres, the precursors were further calcined at 450 ℃ for 8 h with a temperate rate of 2 ℃ min^{-1}.

Material characteristics

The crystallographic information of the mesoporous $ZnCo_2O_4$ microspheres was investigated by powder X-ray diffraction (XRD, PANalytical X'Pert PRO) with Cu-Kα radiation (λ = 1.5604nm) at a scanning rate of 0.02° s^{-1} in the range of 2θ = 10°-80°. The surface elemental compositions of the mesoporous $ZnCo_2O_4$ microspheres was examined by Energy Dispersive Spectrometer (EDS). The thermal gravity analysis (TGA/DTG) measurements of the mesoporous $ZnCo_2O_4$ microspheres was carried out at a heating rate of 10 ℃ min^{-1} from room temperature to 600 ℃ . The morphologies and microstructures of samples were characterized by scanning electron microscopy (SEM, ZEISS ULTRA55) and transmission electron microscopy (TEM, JEM-2100HR), respectively. The Brunauer-Emmett-Teller (BET) specific surface area of the mesoporous $ZnCo_2O_4$ microspheres was calculated using the BET equation. Desorption isotherm was used to determine the pore size distribution using the Barrett-Joyner-Halenda (BJH) method.

The electrochemical performance of samples were measured using CR2430 button cell with lithium serving as the counter and reference electrode assembled in an argon-filled glove box. The working electrode was a composition of 80wt.% active material, 10wt.% acetylene black and 10wt.% PVDF on the copper foil of 10μm thickness, dried at 60 ℃ for 8 h and subsequently pressed. The electrolyte consisted of a solution of 1M LiPF6 in ethylene carbonate (EC), diethyl carbonate (DEC) and ethyl methyl carbonate (EMC) (1:1:1 in volume ratio). The charge/discharge test was conducted with NEWARE Battery Testing System in the Voltage range of 0.01-3.0 V at room temperature. The Cyclic voltammertry (CV) was measured by Solartron 1470E electrochemistry at a scan rate of 0.1 mV s^{-1} between 0.01 V and 3.0 V.

Result and discussion

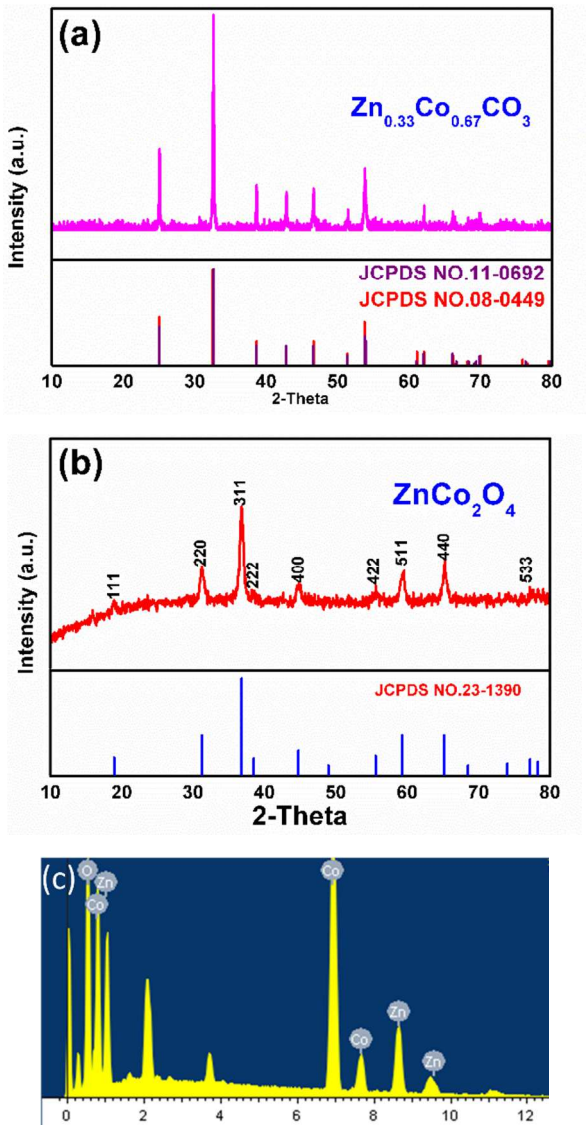

Fig. 2 XRD patterns of the precursors and as-prepared $ZnCo_2O_4$; EDS microanalysis of the samples.

The composition of the precursors were first examined by XRD, and the results (as shown in Fig. 2a) reveal that all the peaks can be indexed to calcite $CoCO_3$ (JCPDS NO.11-0692) and

$ZnCO_3$ (JCPDS NO.08-0449), which indicates the precursors made up of $CoCO_3$ or $ZnCO_3$. Combined with the EDS result (Co:Zn=2.04:1), We can confirm the precursor is $Zn_{0.33}Co_{0.67}CO_3$. The crystallinity and phase information of the samples was provided by the XRD, confirming the formation of single-phase $ZnCo_2O_4$. As indicated in Fig. 2b, all diffraction peaks of the sample observed from the XRD pattern are in good agreement with cubic $ZnCo_2O_4$ spinel structure (α =8.095 Å; space group Fd-3m(227), JCPDS card no.23-1390). The diffraction peaks located at 2 theta of 18.93 °, 31.23 °, 36.81 °, 38.19 °, 44.79 °, 55.59 °, 59.55 °, 65.25 ° and 77.19 ° are corresponded to (111), (220), (311), (222), (400), (422), (511), (440) and (533) crystal planes, respectively. Absence of any diffraction peak of cobalt oxide or ZnO, confirmed the high purity of the samples. The narrow diffraction peaks are indexed to the high crystallinity of the mesoporous $ZnCo_2O_4$ microspheres. Additionally, the EDS information of the as-prepared products was shown in Fig. 2c. The elements of Zn, Co, O could be seen clearly and the other signal come from the SEM substrate. The molar ratio of Zn and Co was detected to be about 1:2.04, which agrees well with the theory ratio. Thus, we reasonable speculate that the XRD patter, combined with the EDS pattern, could confirm the synthesis of $ZnCo_2O_4$.

The thermal properties of the $Zn_{0.33}Co_{0.67}CO_3$ precursor was characterized by the TG measurement. As shown in Fig. 3, there are two major weight loss steps: a gradual weight loss below 280 ℃ is attributed to the loss of free water, EG or other organic molecules. The main weight loss of 32.19 % between 280 and 380 ℃, corresponding to a sharp exothermic peak located at 356.5 ℃ in the DTG curve, originates from the thermal decomposition of the $Zn_{0.33}Co_{0.67}CO_3$ into $ZnCo_2O_4$ by the release of CO_2, as described in Fig. 1. Furthermore, the calculated value is comparable to the theoretical value (31.95 %) of weight loss. No weight loss and exothermic peaks are found over 380 ℃, indicating that the $Zn_{0.33}Co_{0.67}CO_3$ is transformed into $ZnCo_2O_4$ completely. Thus, 450 ℃ was chosen as the calcination temperature for the synthesis of the mesoporous $ZnCo_2O_4$ microspheres.

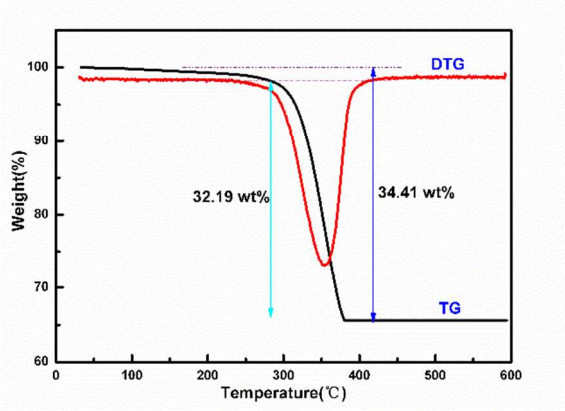

Fig. 3 TG/DTG curves for the $Zn_{0.33}Co_{0.67}CO_3$ precursor.

The detailed morphological and microstructure of the mesoporous $ZnCo_2O_4$ microspheres were investigated by SEM and TEM. From the SEM images shown in Fig. 4a and b, it can be discovered easily that the products is composed of uniform spheres with an average diameter of 6-8 μm. A large amount of pores appears in the microspheres, which rooted in the generation of CO_2 during the decomposition of the precursor. Fig. 4c and d shows the image of a broken microsphere and the high magnification SEM of the section. It reveals that the microstructure of a $ZnCo_2O_4$ sphere is made up of closely packed primary nanoparticles with diameter of about 30 nm. As marked with the red arrow, the calculated size of pores are ranging from 10 to 40 nm, which match well with the result of desorption pore size distribution (Fig. 5). When used as anode materials, as shown in Fig. 4c, the Li^+ ions can diffuse into/out the $ZnCo_2O_4$ microspheres through these pores with little resistance and shot distance. Also, the adequate free space could buffer the volume changes during the charge/discharge process. A representative high-resolution TEM (HRTEM) image is shown in Fig. 4e, which further proves the good crystallinity of the products for its distinct lattice fringes. The HRTEM image (inset pictures in Fig. 4e) reveals three sets of lattice fringes with interplanar spacing of 0.23, 0.24 and 0.28 nm, corresponding to the (222), (311) and (220) plane of spinel crystalline $ZnCo_2O_4$, respectively. The selected area election diffraction (SAED) pattern (Fig. 4f) indicates the polycrystalline nature of the mesoporous $ZnCo_2O_4$ microspheres, and all the diffraction can be indexed as (111), (220), (311), (400), (511) and (440) planes from the inside out, respectively.

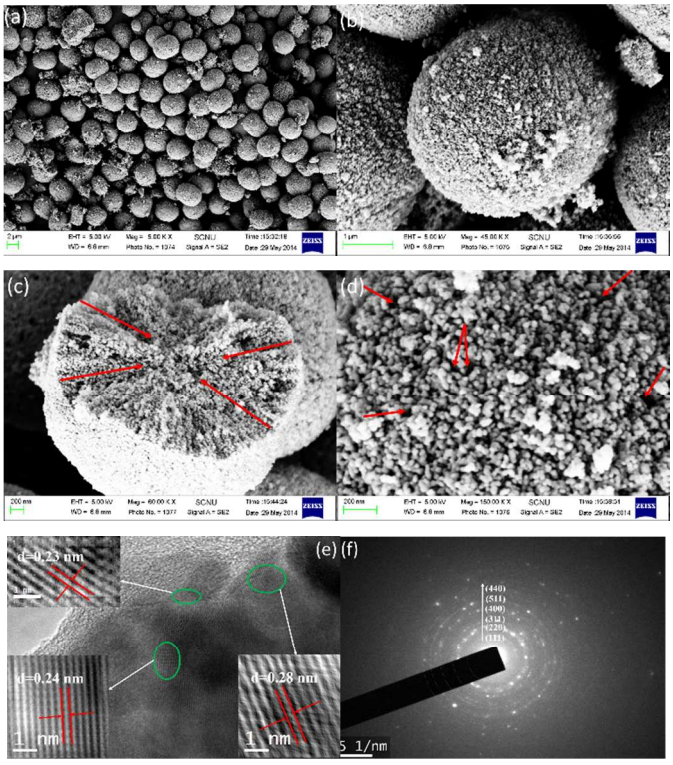

Fig. 4 Characterization of the mesoporous $ZnCo_2O_4$ microspheres: (a-d) SEM images, (e) high-resolution TEM images, (f) SAED.

Specific surface areas of the as-prepared $ZnCo_2O_4$ microspheres was characterized by BET using nitrogen adsorption-desorption isotherm at 200 ℃ for 24 h. From the result (Fig. 5), the isotherm could be categorized as a type Ⅳ with a H1 hysteresis loop (according to the IUPAC classification) at the relative pressure range of 0.9-1.0, implying a mesoporous architectural style of the obtained $ZnCo_2O_4$ microspheres. According to the corresponding Barrett-Joyner-Halenda (BJH) plots (the inset of Fig. 5) calculated nitrogen isotherms, the pore size distribution is in the range of 10-40 nm with an average diameter of about 28 nm, which is in accord with size distribution observed in SEM image. In addition, the mesoporous $ZnCo_2O_4$ microspheres exhibits a relatively high BET surface area of 39.52 m^2 g^{-1} and a pore volume of 0.214 cm^3 g^{-1}. The high surface area is mainly attributable to the unique nanostructure and big total pore volume. It is known well that more locations and channels can be provided by a large surface area for fast Li^+ ion insertion/extraction into the electrode material. Furthermore, the enough pore volume may be beneficial for the Li^+ ion to diffuse efficiently to active material with less resistance and also can buffer the volume expansion during the discharge/charge process. Thus, the obtained $ZnCo_2O_4$ microspheres is expected to improve the electrochemical performance.

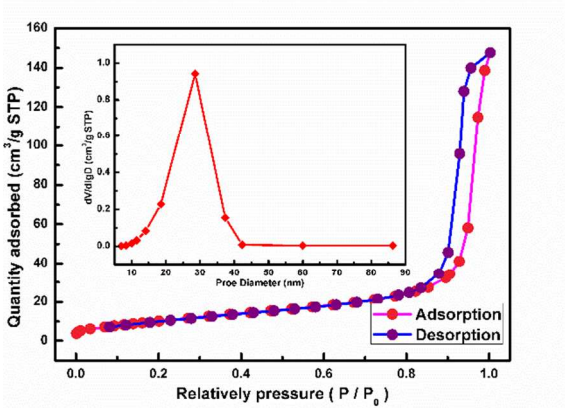

Fig. 5 Nitrogen adsorption-desorption isotherm and the corresponding pore size distribution (inset) of the $ZnCo_2O_4$ microspheres

Motivated by the especially structure, the mesoporous $ZnCo_2O_4$ microspheres was configured as a CR2430 coin cell to investigate the electrochemical properties. The first five cyclic voltammetry (CV) curves of the $ZnCo_2O_4$ electrode (Fig. 6a) at a scan rate of 0.1mVs^{-1} in the voltage range of 0.01-3.0 V. In the first cycle, a broad reduction peak is recorded at 0.42 V, which correspond to the reduction reaction of $ZnCo_2O_4$ to Zn and Co with the formation of Li_2O. In the anodic sweep, two main oxidation peaks located at around 1.7 V and 2.1 V were attributed to the oxidation of Zn and Co to Zn^{2+} and Co^{3+}, respectively. [33] A very weak peak observed at 0.9V (the inset in Fig. 6a) arises from the dealloying process of Li-Zn alloy. The main reduction peak at 0.42 V in the initial cycle was shifted to 0.87 V originated from irreversible reduction reaction and less or no formation of SEI film,[25, 30] while the two main oxidation peaks were barely shift. In addition, the reduction and oxidation peaks in the CV cures overlapped substantially from the second cycle, indicating that the electrode made from the mesoporous $ZnCo_2O_4$ microspheres showed outstanding cyclability for LIBs. According to the previous analysis, the lithium insertion and extraction reaction for the $ZnCo_2O_4$ electrode can be believed to proceed as follows:

$ZnCo_2O_4 + 8Li+ + 8e^- \rightarrow Zn + 2Co + 4Li_2O$ (1)

$Zn + Li^+ + e^- \leftrightarrow LiZn$ (2)

$Zn + Li_2O \leftrightarrow 2Li + ZnO + 2e^-$ (3)

$2Co + 2Li_2O \leftrightarrow 2CoO + 4Li^+ + 4e^-$ (4)

$2CoO + 2/3Li_2O \leftrightarrow 2/3Co_3O_4 + 4/3Li+ +4/3e^-$ (5)

Fig. 6b presents the selected discharge/charge cycle profiles of the electrode made from the mesoporous $ZnCo_2O_4$ microspheres at a current density of 100 mA g^{-1} in a potential window between 0.01 and 3.0 V (vs. Li^+/Li). From the profiles, it can be discovered that there is a clear potential plateau at about 0.9 V in the first discharge curve, and this potential plateau shifts upward close to 1.2 V and becomes steeper in the subsequent discharge curves, which is associated with the above CV detection results. The initial discharge and charge capacities are 1600 and 1205 mAh g^{-1}, leading to a high initial coulombic efficiency of about

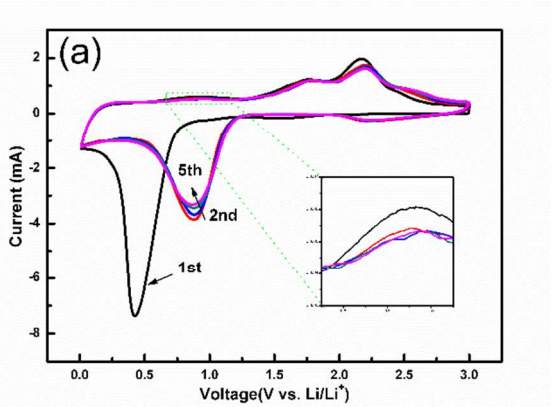

Fig. 6 (a) First five cycles of CVs for the $ZnCo_2O_4$ microspheres at a scan rate of 0.1 mV s^{-1} in the voltage of 0.01-3.0 V

75.3%. Compared with the theoretical value (975 mAh g^{-1}) based on the conversion reaction (eq. 1), the excess capacities (about 625 mAh g^{-1}) can be mainly ascribed to the formation of SEI film and the organic polymeric/gel-like layer.[34,35] Furthermore, the interfacial storage originated from the porous architecture is also considered to be responsible for the extra capacity. The irreversible capacity loss of 24.7% in the initial is assigned to the phenomenon that the formed SEI film cannot

completely decompose during the first charge or the crystal structure destruction/amorphization. [36-38] In addition, there is a large deviation in potential between discharge and charge cures, which is a commonly feature of a large number of metal oxide anodes due to the polarization related to ion transfer during cycling process. [39] The large gap between charge and discharge curves involves the energy efficiency and this phenomenon may result from the poor electrical conductivity of metal oxide anode. [40]

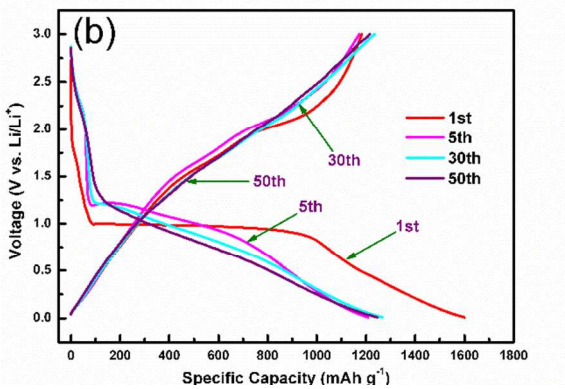

Fig. 6 (b) Discharge-charge profiles of the $ZnCo_2O_4$ microspheres cycled at a constant current of 100 mA g^{-1} in 0.01-3.0 V

The cycling performance and the corresponding coulombic efficiency of the designed mesoporous $ZnCo_2O_4$ microspheres electrode at a current density of 100 mA g^{-1} in the range of 0.01-3.0 V is given in Fig. 6c. The discharge capacities obtained for the first and second cycles are 1600 and 1215 mAh g^{-1}, respectively. Moreover, the as-prepared mesoporous $ZnCo_2O_4$ microspheres presents excellent cyclic capacity retention upon prolonged cycling after the second cycle. From the 5th cycle onward, it is interesting to note that the reversible capacities begin to increase slight during the cycling and a reversible capacity as high as 1256 mAh g^{-1} retained at the end of 100 cycles, which is a bit higher than the reversible capacity of the second cycle (1215 mAh g^{-1}). This interesting phenomenon may be attributed to more electrolyte gradually penetrating into inner part of active materials through numerous porous in the sample during the Li^+ insertion/extraction process. On the other hand, the progressive generation of electrode-chemistry active polymeric gel-like films may also contribute to the increasing reversible capacity. Beside the superior specific capacity and excellent cyclability, the rate capability is another important parameter for many practical applications of LIBs such as electric vehicles and power tools. The rate capability of the mesoporous $ZnCo_2O_4$ microspheres electrode was evaluated at various current densities from 500 to 4000 mAh g^{-1}. As shown in Fig. 6d, the average discharge capacity decreases from 1103, 1000, 760 and 430 mAh g^{-1} when the current density was gradually increased from 500 to 1000, 2000 and 4000 mA g^{-1}. In the subsequent cycle, the specific capacities rebound to 530, 670 and 900 mAh g^{-1} with the current densities back to 2000, 1000 and 500 mA g^{-1}, respectively. This result demonstrates that the mesoporous $ZnCo_2O_4$ microspheres has great potential as a high rate anode material for LIBs.

Because the mesoporous $ZnCo_2O_4$ microspheres shows an excellent rate capacity, we further evaluated the electrochemical performance of the $ZnCo_2O_4$ electrode at a high current density. As shown in Fig. 7, the discharge capacity decreased from the initial capacity of 1366 mAh g^{-1} rapidly to 645 mAh g^{-1} after 75 cycles when a high density of 1000 mA g^{-1} was applied to the $ZnCo_2O_4$ electrode. The reason for the capacity decreasing rapidly may be that the continuous loss of active materials would occur at a high rate due to the embedding of metallic cobalt and zinc in Li_2O matrix partially. Besides, the structure strain of the mesoporous $ZnCo_2O_4$ microspheres would be inevitable during the discharge/charge process even though the mesoporous $ZnCo_2O_4$ microspheres provide enough free space to buffer the volume expansion, which lead to a part of active materials failure. However, the discharge capacity slowly increased to 774 mAh g^{-1} after 200 cycles. The result is greatly superior to the lately report in which the $ZnCo_2O_4$ has a discharge capacity of 432 mAh g^{-1} after 40 cycles and 331 mAh g^{-1}, 202 mAh g^{-1} after 500 cycles.[41,42] In addition, the mesoporous $ZnCo_2O_4$ microspheres also shows the outstanding electrochemical performance as anode materials for LIBs compared to other cobalt-based spinel structure. For example, the discharge capacity of $MnCo_2O_4$ microspheres just retained 320 mAh g^{-1} after 200 cycles at 900 mA g^{-1} and the mesoporous $NiCo_2O_4$ microspheres stabilized at 705 mAh g-1 after 500 cycle at a current density of 800 mA g^{-1}.[43, 44] The excellent cyclic performance of mesoporous $ZnCo_2O_4$ microspheres at a high density was further demonstrated the great potential as a high rate anode material for LIBs.

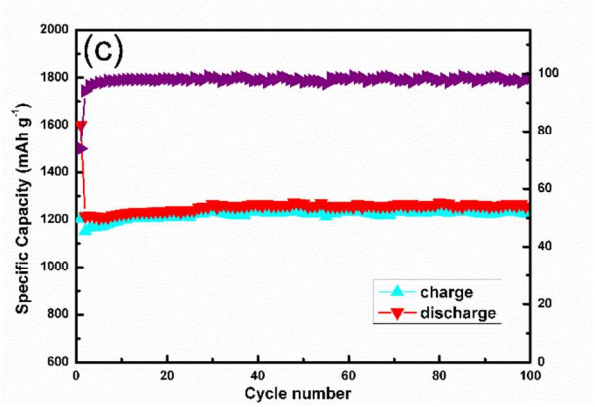

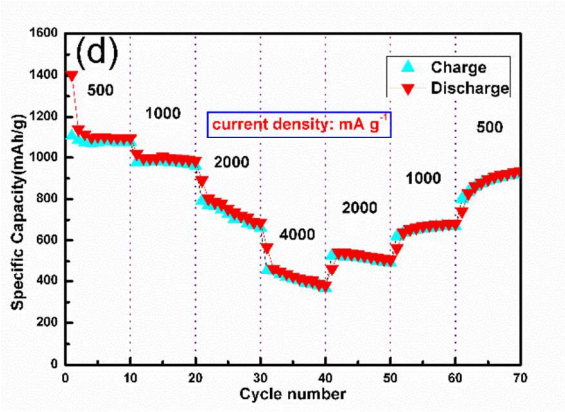

Fig. 6 (c) Cycling performance of as-prepared $ZnCo_2O_4$ ectrodes for the first 100 cycles and the corresponding coulombic efficiency at a constant current of 100 mA g^{-1}, (d) Rate performance of the $ZnCo_2O_4$ electrode.

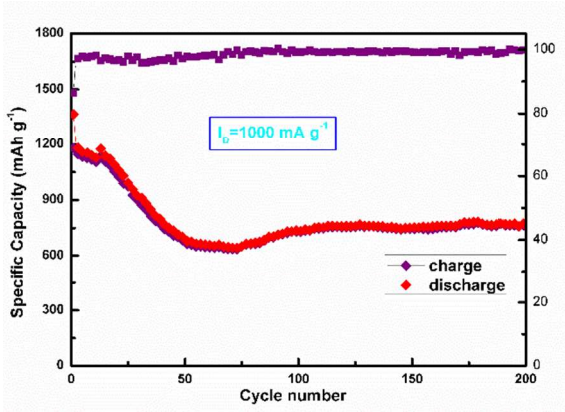

Fig. 7 Cycling performance of as-prepared $ZnCo_2O_4$ ectrodes at a high density current of 1000 mA g^{-1}.

Conclusions

In summary, we have developed a facile hydrothermal method to prepare the uniform the mesoporous $ZnCo_2O_4$ microspheres by pyrolysis of the $Zn_{0.33}Co_{0.67}CO_3$ precursor at 450 ℃in air. The obtained mesoporous $ZnCo_2O_4$ microspheres possesses high surface area and provides a large amount of mesopores. The large surface area permits a high interfacial contact area with the electrolyte and provides more locations and channels for fast Li^+ into insertion/extraction into the electrode material. The porous structure may not only be beneficial for Li^+ ion to diffuse efficiently to active material with less resistance but also buffer the volume expansion during the discharge/charge process. When used as an anode material for LIBs, the specific capacity still maintains a high value of 1256 mAh g^{-1} after 100 cycles at a current density of 100 mA g^{-1} in the potential ranging from 0.01 to 3.0 V, which is about 3.4 times larger than that of the commercial graphite electrode (372 mAh g^{-1}). More interesting, the reversible capacity as high as 774 mAh g^{-1} can be retained at a high current density of 1000 mA g^{-1} after 200 cycles, which indicates that the mesoporous $ZnCo_2O_4$ microspheres has the potential to be a high rate anode material for LIBs. Based on the facile synthetic method and excellent electrochemical properties, the mesoporous $ZnCo_2O_4$ microspheres will hold the promise for the next-generation high power LIBs.

Acknowledgements

This work was supported by National Natural Science Foundation of China (Grant No. 51101062 and 51171065), Science and Technology Project of Guangzhou City, China (Grant No. 2011J4100075), Foundation for Distinguished Young Talents in Higher Education of Guangdong, China (Grant No. LYM09052), China Scholarship Council (No. 201308440314), Extracurricular Science Foundation for Students in South China Normal University of Guangdong, China (Grant No. 13WDGB03), The Scientific Research Foundation of Graduate School of South China Normal University (Grant No. 2013KYJJ039), The Natural Science Foundation of Guangdong province (Grant No. S2012020010937, 10351063101000001), and University-Industry Cooperation Projects of Guangdong province, Ministry of Education and Science & Technology (Grant No. 2011A091000014).

Notes and references

[a] School of Physics and Telecommunication Engineering, South China Normal University, Guangzhou 510006，PR China.
[b] Engineering Research Center of Materials and Techcccccnology for Electrochemical Energy Storage (Ministry of Education), Guangzhou 510006, PR China.
[c] Laboratory of Quantum Engineering and Quantum Materials, School of Physics and Telecommunication Engineering, South China Normal University, Guangzhou 510006, PR China.
*Corresponding author Tel: +86-20-39318011
E-mail addresses: rq7702@yeah.net (Q. Ru)

† Footnotes should appear here. These might include comments relevant to but not central to the matter under discussion, limited experimental and spectral data, and crystallographic data.

Electronic Supplementary Information (ESI) available: [details of any supplementary inccformation available should be included here]. See DOI: 10.1039/c000000x/

1 P. Poizot, S. Laruelle, S. Grugeon, L. Dupont and J. M. Tarascon, *Nature*, 2000, **407**, 496-499.
2 L. W. Ji, Z. Lin, M. Alcoutlabi and X. W. Zhang, *Energy Environ. Sci.*, 2011, **4**, 2682-2699.
3 H. L. Wang, L. F. Cui, Y. Yang, H. S. Casalongue, J. T. Robinson, Y. Y. Liang, Y. Cui and H. J. Dai, *J. Am. Chem. Soc.*, 2010, **132**, 13978-13980.
4 Y. G. Li, B. Tan and Y. Y. Wu, *Nano Lett.*, 2008, **8**, 265-270.
5 J. M. Tarascon and M. Armand, *Nature*, 2001, **414**, 359-367.
6 X. S. Zhou, Y. X. Yin, L. J. Wan and Y. G. Guo, *Chem. Commun.*, 2012, **48**, 2198-2200.

7 W. M. Zhang, J. S. Hu, Y. G. Guo, S. F. Zheng, L. S. Zhong, W. G. Song and L. J. Wan, *Adv. Mater.*, 2008, **20**, 1160-1165.
8 L. Qie, W. M. Chen, Z. H. Wang, Q. G. Shao, X. Li, L. X. Yuan, X. L. Hu, W. X. Zhang and Y. H. Huang, *Adv. Mater.*, 2012, **24**, 2047-2050.
9 J. Chen, X. H. Xia, J. P. Tu, Q. Q. Xiong, Y. X. Yu, X. L. Wang and C. D. Gu, *J. Mater. Chem.*, 2012, **22**, 15056-15061.
10 Y. F. Deng, Q. M. Zhang, Z. C. Shi, L. J. Han, F. Peng and G. H. Chen, *Electrochim. Acta*, 2012, **76**, 495-503.
11 A. K. Mondal, D. W. Su, Y. Wang, S. Q. Chen and G. X. Wang, *Chem. Asian J.*, 2013, **8**, 2828-2832.
12 L. Zhang, H. B. Wu, R. Xu and X. W. (David) Lou, *CrystEngComm.*, 2013, **15**, 9332-9335.
13 N. Jayaprakash, W. D. Jones, S. S. Moganty and L. A. Archer, *J. Power Sources*, 2012, **200**, 53-58.
14 J. Y. Wang, N. L. Yang, H. J. Tang, Z. H. Dong, Q. Jin, M. Yang, D. Kisailus, H. J. Zhao, Z. Y. Tang and D. Wang, *Angew. Chem.*, 2013, **125**, 6545-6548.
15 H. Long, T. L. Shi, S. L. Jiang, S. Xi, R. Chen, S. Y. Liu, G. L. Liao and Z. R. Tang, *J. Mater. Chem. A*, 2014, **2**, 3741-3748.
16 X. Song, Q. Ru, B. B. Zhang, S. J. Hu and B. N. An, *J. Alloys Comp.*, 2014, **585**, 518-522.
17 C. Liang, M. X. Gao, H. G. Pan, Y. F. Liu and M. Yan, *J. Alloys Comp.*, 2013, **575**, 246-256.
18 Z. L. Zhang, Y. H. Wang, D. Li, Q. Q. Tan, Y. F. Chen, Z. Y. Zhong and F. B. Su, *Ind. Eng. Chem. Res.*, 2013, **52**, 14906-14912.
19 Y. Sharma, N. Sharma, G. V. Subba Rao and B. V. R. Chowdari, *Solid State Ionics*, 2008, **179**, 587-597.
20 Y. J. Chen, J. Zhu, B. H. Qu, B. G. Lu and Z. Xu, *Nano Energy*, 2014, **3**, 88-94.
21 T. Y. Wei, C. H. Chen, H. C. Chien, S. Y. Lu and C. C. Hu, *Adv. Mater.*, 2010, **22**, 347-351.
22 W. Luo, X. Hu, Y. Sun and Y. Huang, *J. Mater. Chem.*, 2012, **22**, 8916-8921.
23 Y. C. Qiu, S. H. Yang, H. Deng, L. M. Jin and W. S. Li, *J. Mater. Chem.*, 2010, **20**, 4439-4444.
24 B. Liu, X. F. Wang, B. Y. Liu, Q. F. Wang, D. S. Tan, W. F. Song, X. J. Hou, D. Chen and G. Z. Shen, *Nano Res.*, 2013, **6**, 525-534.
25 N. Du, Y. F. Xu, H. Zhang, J. X. Yu, C. X. Zhai and D. R. Yang, *Inorg. Chem.*, 2011, **50**, 3320-3324.
26 B. Liu, J. Zhang, X. Wang, G. Chen, D. Chen, C. Zhou and G. Shen, *Nano Lett.*, 2012, **12**, 3005-3011.
27 H. W. Liu and J. Wang, *Electrochim. Acta*, 2013, **92**, 371-375.
28 D. Deng and J. Y. Lee, *Nanotechnology*, 2011, **22**, 355401-355409.
29 Q. S. Xie, F. Li, H. Z. Guo, L. S. Wang, Y. Z. Chen, G. H. Yue and D. L. Peng, *Appl. Mater. Interfaces*, 2013, **5**, 5508-5517.
30 Y. Sharma, N. Sharma, G. V. S. Rao and B. V. R. Chowdari, *Adv. Funct. Mater.* 2007, **17**, 2855-2861.
31 T. Wei, Y. Y. Hou, F. X. Wang, L. L. Liu, Y. P. Wu and K. Zhu, *Nano Lett.* 2013, **13**, 2036-2040.
32 F. X. Wang, S. Y. Xiao, Z. Chang, Y. Q. Yang and Y. P. Wu, *Chem. Comm.*, 2013, **49**, 9209-9211.
33 N. Du, Y. F. Xu, H. Zhang, J. X. Yu, C. X. Zhai and D. R. Yang, *Inorg. Chem.*, 2011, **50**, 3320-3324.
34 N. Munichandraiah, L. G. Scanlon and R. A. Marsh, *J. Power Sources* 1998, **72**, 203-210.
35 S. Laruelle, S. Grugeon, P. Poizot, M. Dolle, L. Dupont and J. M. Tarascon, *J. Electrochem. Soc.*, 2002, **149**, A627-A634.
36 M. V. Reddy, B. L. Wei Wen, K. P. Loh and B. V. R. Chowdari, *ACS Appl. Mater. Interfaces*, 2013, **5**, 7777-7785.
37 M. V. Reddy, C. Yu, F. Jiahuan, K. P. Loh and B. V. R. Chowdari, *ACS Appl. Mater. Interfaces*, 2013, **5**, 4361-4366.
38 M. V. Reddy, L. Y. T. Andreea, A. Y. Ling, J. N. C. Hwee, C. A. Lin, S. Admas, K. P. Loh, M. K. Mathe, K. I. Ozoemena and B. V. R. Chowdari, *Electrochim. Acta*, 2013, **106**, 143-148.
39 Y. J. Mai, S. J. Shi, D. Zhang, Y. Lu, C. D. Gu and J. P. Tu, *J. Power Sources*, 2012, **204**, 155-161.
40 Y. J. Mai, X. H. Xia, R. Chen, C. D. Gu, X. L. Wang and J. P. Tu, *Electrochim. Acta*, 2012, **67**, 73-78.
41 L. L. Hu, B. H. Qu, C. C. Li, Y. J. Chen, L. Mei, D. N. Lei, L. B. Chen, Q. H. Li and T. H. Wang, *J. Mater. Chem. A*, 2013, **1**, 5596-5602.
42 J. F. Li, J. Z Wang, D. Wexler, D. Q. Shi, J. W. Liang, H. K. Liu, S. L. Xiong and Y. T. Qian, *J. Mater. Chem. A*, 2013, **1**, 15292-15299.
43 C. C. Fu, G. S. Li, D. Luo, X. S. Huang, J. Zheng and L. P. Li, *ACS Appl. Mater. Interfaces*, 2014, **6**, 2439-2449.
44 J. F. Li, S. L. Xiong, Y. R. Liu, Z. C. Ju and Y. T. Qian, *ACS Appl. Mater. Interfaces*, 2013, **5**, 981-988.

The as-prepared mesoporous ZnCo2O4 microspheres shows a high specific capacity and excellent electrochemical performance when used as an anode material for LIBs.